Journal of Biomechanics 93 (2019) 60–69

Contents lists available at ScienceDirect

Journal of Biomechanics

journal homepage: www.elsevier.com/locate/jbiomech
www.JBiomech.com

A quasi three-dimensional visualization of unsteady wake flow in human undulatory swimming

Hirofumi Shimojo [a,b,*], Tomohiro Gonjo [c], Jun Sakakibara [d], Yasuo Sengoku [e], Ross Sanders [f], Hideki Takagi [e]

[a] Faculty of Health Science, Department of Health and Sports, Niigata University of Health and Welfare, Japan
[b] Institute for Human Movement and Medical Sciences, Niigata University of Health and Welfare, Japan
[c] Department of Physical Performance, Norwegian School of Sport Sciences, Norway
[d] Department of Mechanical Engineering, Meiji University, Japan
[e] Faculty of Health and Sport Sciences, University of Tsukuba, Japan
[f] Faculty of Health Sciences, The University of Sydney, Australia

ARTICLE INFO

Article history:
Accepted 14 June 2019

Keywords:
PIV
Dolphin kick
Motion analysis
Water flume

ABSTRACT

Human undulatory underwater swimming (UUS) is an underwater propelling technique in competitive swimming and its propulsive mechanism is poorly understood. The purpose of this study was to visualize the three-dimensional (3D) flow field in the wake region during human UUS in a water flume. A national level male swimmer performed 41 UUS trials in a water flume. A motion capture system and stereo particle image velocimetry (PIV) equipment were used to investigate the 3D coordinates of the swimmer and 3D flow fields in the wake region. After one kick cycle was divided into eight phases, we conducted coordinate transformations and phase averaging method to construct quasi 3D flow fields. At the end of the downward kick, the lower limbs external rotations of the lower limbs were observed, and the feet approached towards each other. A strong downstream flow, i.e. a jet was observed in the wake region during the downward kick, and the paired vortex structure was accompanied by a jet. In the vortex structure, a cluster of vortices and a jet were generated in the wake during the downward kick, and the vortices were subsequently shed from the feet by the rotated leg motion. This suggested that the swimmer gained a thrust by creating vortices around the foot during the downward kick, which collided to form a jet. This paper describes, illustrates, and explains the propulsive mechanism of human UUS.

1. Introduction

Examining undulatory underwater swimming (UUS), which is an underwater propelling technique in competitive swimming used during the start and turn phases, has become a popular research topic (Andersen and Sanders, 2018; Arellano et al., 2002; Cohen et al., 2012; Connaboy et al., 2009; Hochstein and Blickhan, 2011; Miwa et al., 2006; Pacholak et al., 2014; von Loebbecke et al., 2009). In animal locomotion, there are two fundamental principles of propulsion. Firstly, hydrodynamic forces are generated by transferring momentum to the environment through repetitive motion such as body undulations or oscillation of appendages (legs, fins, or wings), and secondly, the locomotor speed is modulated by controlling the amplitude and frequency of the periodic motion (Biewener, 2003). These principles can also be applied to human UUS. However, swimmers can produce different UUS speed with similar kinematics due to a dissimilar ability to control the vortices produced (Arellano et al., 2002; Connaboy et al., 2009; Ungerechts et al., 1998).

To investigate the fluid dynamics of human UUS, computational fluid dynamics (CFD) and particle image velocimetry (PIV) methods have been used. CFD is a numerical simulation technique for solving the Navier–Stokes equations of fluid flow (Ferziger and Perić, 2012). Some studies simulated the flow around an entire body performing UUS using CFD (Cohen et al., 2012; Pacholak et al., 2014; von Loebbecke et al., 2009) and demonstrated maximum thrust being generated during downward kicking. These CFD studies have also shown three-dimensional (3D) vortex rings in the wake region after the downward kick. On the other hand, PIV is a flow visualization method to measure instantaneous velocities and related phenomena such as normal and shear stress in the

* Corresponding author at: Faculty of Health Science, Department of Health and Sports, Niigata University of Health and Welfare, 1398 Shimami-cho, Kita-ku, Niigata-shi, Niigata, 950-3198, Japan.
E-mail address: shimojo@nuhw.ac.jp (H. Shimojo).

https://doi.org/10.1016/j.jbiomech.2019.06.013
0021-9290/

flow. Two-dimensional (2D) vortex structure has been observed in human UUS using PIV (Hochstein and Blickhan, 2011; Miwa et al., 2006). Also, Pacholak et al. (2014) showed 3D vortex rings using a CFD method based on the previously captured swimmer's kinematics parameters of Hochstein and Blickhan (2011). However, no research has demonstrated a full 3D vortex structure in human swimming using PIV.

PIV has been used to study the locomotion of fish, and 3D vortex structure in the wake region has been observed (Drucker and Lauder, 1999; Flammang et al., 2011; Sakakibara et al., 2004). However, these hydrobiological observation areas were set at 200–300 mm^2, which is too small for observing the wake region in human swimming. To our knowledge, only two studies have been conducted to visualize flow on a large scale using PIV (Fish et al., 2014; Fish et al., 2018). The researchers visualized flow fields and vortex structures in the wake region of actual dolphin swimming with the observation area of 1.0 m^2, however, it was limited to 2D analysis of flow fields. In addition, sequential PIV has been used in human swimming (Matsuuchi et al., 2009; Miwa et al., 2006), which has a low time resolution with a time duration of 67–100 ms because the laser sheet illuminates a large region with high pulse energy. Furthermore, multiple trials were necessary to capture the critical instants of vortex creation with the use of sequential PIV. Applying a 2D approach, Fish et al. (2014) estimated, from the vortex circulation (Weihs, 1972), that the thrust produced by a dolphin ranged from 50 N to 1467 N. However, the values obtained using 2D flow fields would contain some error because of the dolphin's tail, and its motion, are three dimensional.

PIV experimentation is typically constrained by low spatial and temporal resolution. To overcome these constraints, Imamura and Matsuuchi (2013) visualized quasi 3D flow fields in the wake of a wing oscillating in a water flume by sampling multiple cross sections of the flow field. The authors calculated the propulsive forces from the temporal variations in circulation of a vortex ring. This quasi 3D flow fields approach was an epoch-making idea because complete 3D flow fields had been realized by a tomographic PIV method that needs multiple cameras and narrow space, and costly. If 3D flow fields visualization in the wake region during UUS is realized, we can estimate a propulsive force using the circulation equation of a vortex ring without a measurement system such as using sensors (Milne-Thomson, 1966). By using waterproof pressure sensors, although pressure distribution analysis has been established for estimating propulsive force in human breaststroke swimming (Tsunokawa et al., 2015), the propulsive mechanism of the estimated fluid forces could not be explained sufficiently because of the absence of information about the relation the force and unsteady flow around a foot. Thus, this quasi 3D PIV approach, i.e. calculating propulsive forces by vortex circulation in the wake region may be applied to study vortex production by human swimmers to estimate the thrust power. In addition, the description of thrust acquisition with flow pattern changing would bring us an understanding of how the propulsive mechanism is produced in swimming. The purpose of this study was to visualize the quasi 3D flow field in the wake region during human UUS in a water flume. This approach will reveal patterns of vortices in the wake not previously reconstructed from 2D analyses.

2. Methods

2.1. Participants and experimental procedure

A national level male swimmer (age 24 years, height 1.76 m, weight 81.0 kg, FINA point 793) participated in this study. Informed consent was obtained from the swimmer. The present study was conducted in accordance with the tenets of the Declaration of Helsinki and approved by the ethical committee of a university (No. 18072).

The testing was conducted in a water flume (Fig. 1; height 2.0 m, width 1.5 m, length 5.0 m, water temperature was 27 °C). To obtain 3D coordinate data of joints of the swimmer, we used a motion capture system (MOTIVE, Nobby Tech. Ltd., Japan, 18 cameras, sampling frequency 120 Hz). We defined a rectangular cartesian coordinate system, named 'global coordinate', aligning *x*' as the flow direction, *y*' as the horizontal direction perpendicular to the *x*'-direction, and *z*' as vertical direction (Fig. 1a). The origin was 360 mm from the upstream end of the water flume along its centerline.

Stereo PIV was used to visualize the flow in the region of the swimmer's wake. The flow in the flume was seeded with microbubbles (diameter $\approx 50\,\mu m$, the rise velocity was about $10^{-3}\ m{\cdot}s^{-1}$ so that the buoyancy effect is negligibly small) as tracer particles and (Hart, 2000). Center of the laser lightsheet, 4 mm in thickness, was irradiated at *x*' = 8 mm parallel to *y*'-*z*' plane through the bottom window of the flume by a double-pulsed Nd: YAG laser (Quantel Co., Ltd, EverGreen 200, wavelength $\lambda = 532$ nm, maximum power $P = 1$ kW) that can measure instantaneous flow velocity field based on double pulsed laser. Two high-resolution cameras (LaVision Ltd., Imager sCMOS, 2560×2160 pixel) were placed outside the left window of the flume to capture the images of tracer particles visualized by the laser light sheet. The angle between the optical axes of the two cameras was about 90°, and the lenses were mounted to satisfy the Scheimpflug condition that reduces an astigmatism aberration and produces focused image. The swimmer wore laser light protection goggles that remove only the green wavelength, corresponding to the laser to prevent damage of the retinas.

Before the trials, the swimmer performed a warm-up at an indoor pool in close proximity and then practiced UUS in the flume. Since the testing consisted of 41 trials, the flow velocity was set at a moderate intensity of the swimmer ($0.8\ m{\cdot}s^{-1}$) to minimize the effect of fatigue. This velocity was 47.6% of the maximal UUS velocity of the swimmer, and the swimmer did not perceive fatigue at the completion of all trial.

After the warm-up and familiarization, 18 active light-emitting diode (LED) markers were attached on the right and left lower limb anatomical landmarks namely; great trochanter (hip), lateral epicondyle of the femur (knee lateral), medial epicondyle of the femur (knee medial), lateral malleolus (ankle lateral), medial malleolus (ankle medial), calcaneus (heel), head of fifth metatarsal (MP5), head of first metatarsal (MP1) (Fig. 1b).

Ten visible line markers were attached to the bottom window of the flume to enable the swimmer to maintain the instructed position (Fig. 1a) while performing UUS. The same UUS motion was then repeated to obtain 3D flow fields at 41 different positions. The interval between adjacent positions was set at 0.4 m. At each position, the swimmer performed UUS for 15 s that contained 12–20 kick cycles.

2.2. Kinematic analysis

We defined a kick cycle as the duration between the maximum *z*'-displacement of the left MP5 marker and its subsequent maximum during UUS, and the duration of one kick cycle was analyzed. The kick amplitude was computed from the *z*'-displacement of the MP5 over a complete kick cycle. In addition, the displacement and velocity of the MP5 marker and knee joint angle from all trials were obtained because of its key role in the analysis described below. To identify the effect of fatigue and/or the learning effect, we evaluated the variations of kinematics among trials. These kinematic parameters were calculated using MATLAB (Mathworks, USA).

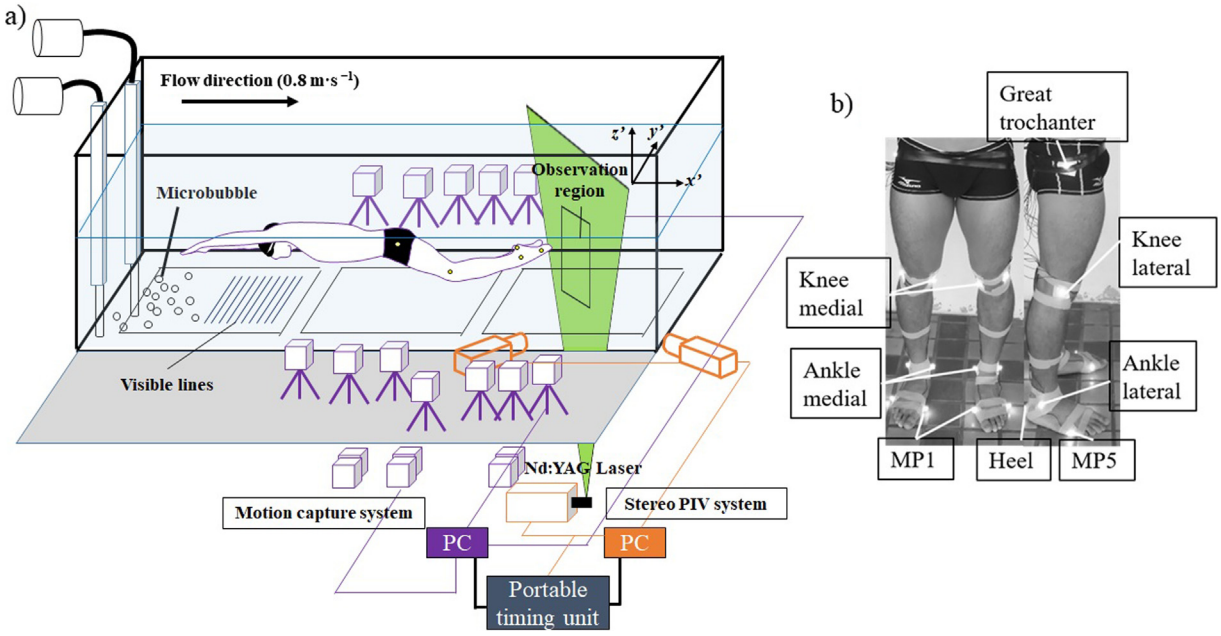

Fig. 1. (a) Experiment set up for motion capture and stereo PIV. (b) A photograph of attached active LED markers at anatomical landmarks.

2.3. Phase definition

Each kick cycle was divided into eight phases (Fig. 2). The upward phase was defined as from the minimum to the subsequent maximum z'-displacement of the left MP5 marker, and the downward phase was the duration between the end of the upward phase and the next minimum z'-displacement of the left MP5. The measured average kick amplitude was 0.72 ± 0.01 m from all trials, and the hip-MP5 difference ranged from −0.4 m to 0.4 m. We separated the two phases into four sub-phases using the hip-MP5 difference in z'-direction (1st −0.4 m to −0.2 m; 2nd −0.2 m to 0.0 m; 3rd 0.0 m to 0.2 m; 4th 0.2 m to 0.4 m).

2.4. Flow visualization

The observational region was set at the swimmer's wake (Fig. 1a). We evaluated particle images by using stereo PIV software DaVis 8.2.0 (LaVision, LaVision Inc. Germany) to obtain the flow velocity field. The stereo PIV requires camera calibration procedures to establish a function between the global coordinate and image coordinates. We recorded images of a calibration plate, which has 0.309 × 0.309 m in dimension equipped with round markers with a specific interval. The calibration plate placed on the laser light sheet plane, and the function based on a pin-hole camera mode was computed through the images.

The location of the calibration plate in the global coordinate was determined from the coordinate of LED markers attached at the edges of the calibration plate, which was captured by the motion capture system. This procedure enabled both PIV and motion capture systems to have the same global coordinate system.

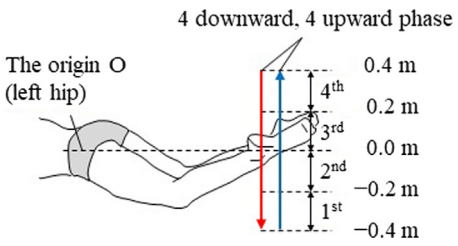

Fig. 2. Phase definition. The left hip marker was used as a reference, and the difference of perpendicular displacement between the hip marker and the left toe marker (MP5) was separated into quartiles (0.2 m).

We used a particle intensity normalization (max/min filter was 5 pixel) in preprocessing. A stereo cross-correlation and a multi-pass interrogation scheme with the decreasing interrogation windows of 128 × 128 and 64 × 64 pixels with 50% overlap was selected. The particle displacement ($\Delta x'$, $\Delta y'$, $\Delta z'$) during a short period of time Δt determined the flow velocity of the particle as

$$u = \frac{\Delta x'}{\Delta t}, v = \frac{\Delta y'}{\Delta t}, w = \frac{\Delta z'}{\Delta t} \quad (1)$$

where (u, v, w) denote the particle velocity components in the x'-, y'-, and z'-directions, respectively. In the present study, Δt was set at 0.3 ms. The stereo-PIV measurement region was rectangular and its dimension was 0.8 × 0.5 m in the y'–z' plane, and areas outside the calibrated space were masked. All the three components of flow velocity were determined at grid points spaced at 14.2 mm ($=\Delta y' = \Delta z'$) in both y'- and z'-direction.

The motion capture system and the flow visualization system were synchronized, and the recording timing was controlled by a portable timing unit (PTU). The time of the pulsed laser (15 Hz) and the motion capture system (120 Hz) were recorded for data synchronization in the analysis (Imamura and Matsuuchi, 2013).

Prior to the swimming trials, the flow field was recorded at steady flow conditions, i.e. without any object or human in the flume at the flow velocity of 0.8 m·s^{-1}. We calculated the coefficients of variance (CV) of the continuous 18 flow fields, i.e. the flow velocity vector data during 1.19 s, and the error in PIV measurements was less than 1%. Before the analysis, steady state flow field data were subtracted from the UUS flow field. When visible noises were observed in the flow fields near the swimmer's foot, these noises were masked manually during the analysis.

2.5. Coordinate transformations and phase averaging

We replicated the procedure of Imamura and Matsuuchi (2013) in the present study.

The measurement planes were displaced relative to the swimmer by changing the swimmer's position in the direction normal to the laser sheet, instead of moving the optical system. In data analysis, we defined another coordinate system (x, y, z), named

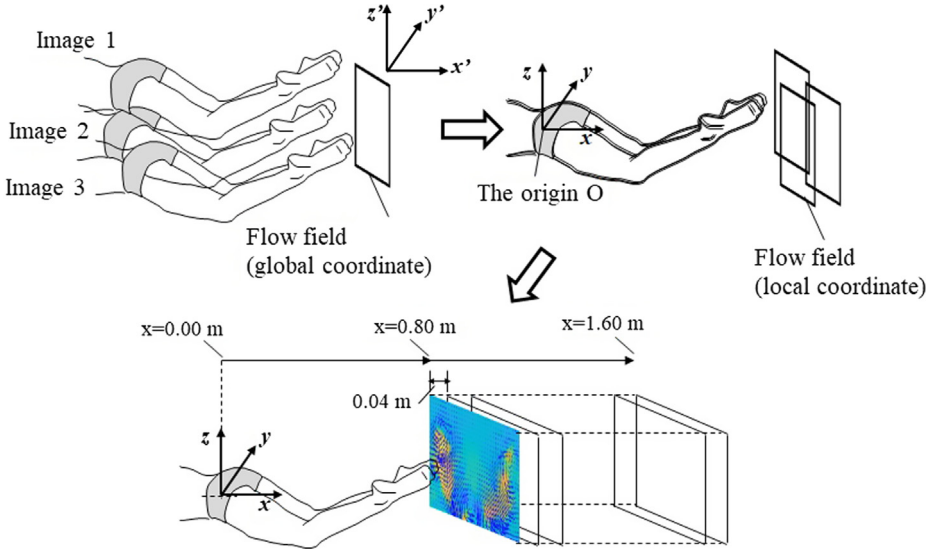

Fig. 3. Typical procedure of converting global to local coordinate system and placing flow fields in the wake region. We selected the flow field from the same phase (e.g. 3rd phase of the downward kick in the figure), then transformed global to local coordinate system by reference to the left hip marker as the origin O. After this, the flow fields were placed in the *x*-direction. The plane is from 0.80 m to 1.60 m in 0.04 m steps from the swimmer's left hip marker as the origin O, and 21 flow fields were used.

'local coordinate', which was parallel to the global coordinate, but has its origin (the origin O), at the left hip marker as shown in Fig. 3. The origin O, which was not fixed in the global coordinate due to the motion of the swimmer's body, was determined by the motion capture system.

The flow velocity vector data, which was defined in the global coordinate system, was transformed into the local coordinate system. The flow velocity data in the local coordinate system was then classified in a series of 21 streamwise bins extending from $x = 0.80$ m to 1.60 m with $\Delta x = 0.04$ m interval (Fig. 3), and also in 8 kicking phase bins (Fig. 2).

Finally, we averaged the flow velocity data both in each streamwise and phase bins to build the reconstructed quasi 3D flow velocity field. The number of realizations in the bin was $n_r = 18.3$ (minimum 1, maximum 82).

The 3D vortex structure was depicted by plotting the *iso*-vorticity surface calculated from the reconstructed flow velocity data. The vorticity components are given by

$$(\omega_x, \omega_y, \omega_z) = \left(\frac{\partial w}{\partial y} - \frac{\partial v}{\partial z}, \frac{\partial u}{\partial z} - \frac{\partial w}{\partial x}, \frac{\partial v}{\partial x} - \frac{\partial u}{\partial y}\right) \quad (2)$$

Three components of the vorticity, ω_x, ω_y, ω_z, and the absolute value ω, defined as

$$\omega = \sqrt{\omega_x^2 + \omega_y^2 + \omega_z^2} \quad (3)$$

were calculated from the reconstructed flow velocity data (Imamura and Matsuuchi, 2013). To smooth the 3D vorticity data, we used a 3D median filter ($3 \times 3 \times 3$) using a MATLAB program.

3. Results

Table 1 shows the kinematic results in the first five trials and selected trials in ten steps. The measured kick cycle count, and the mean and standard deviation (SD) of the one kick cycle duration (s), the kick amplitude (m), the downward kick duration (s), and the upward kick duration (s) among the trials are shown. The CV of 41 trials were 3.61% in kick duration; 1.73% in kick amplitude; 5.31% in downward kick duration; and 2.62% in upward kick duration respectively. Fig. 4 illustrates the position and the velocity of MP5 in the local coordinate system averaged from all trials (613 kick cycles), and Fig. 5 shows the averaged knee angle and CV. The highest value of the knee angle CV was 5.79% in the downward kick, and the lowest value was 0.80% in the upward kick.

Table 1
The kinematic result in first five trials and selected trials in ten steps.

Variables	Trial 1	Trial 2	Trial 3	Trial 4	Trial 5	Trial 11	Trial 21	Trial 31	Trial 41
Measured kick cycle count	18	16	16	16	15	16	14	16	16
Kick duration (s)									
Mean	0.879	0.832	0.851	0.821	0.851	0.818	0.845	0.771	0.821
SD	0.077	0.038	0.040	0.037	0.036	0.021	0.024	0.019	0.026
Kick amplitude (m)									
Mean	0.718	0.710	0.730	0.704	0.736	0.724	0.738	0.710	0.732
SD	0.046	0.029	0.032	0.036	0.041	0.025	0.020	0.019	0.020
Downward kick duration (s)									
Mean	0.386	0.352	0.359	0.343	0.362	0.340	0.351	0.319	0.341
SD	0.063	0.020	0.027	0.016	0.014	0.018	0.017	0.014	0.017
Upward kick duration (s)									
Mean	0.493	0.486	0.492	0.478	0.489	0.478	0.493	0.453	0.481
SD	0.043	0.037	0.019	0.026	0.026	0.012	0.014	0.011	0.017

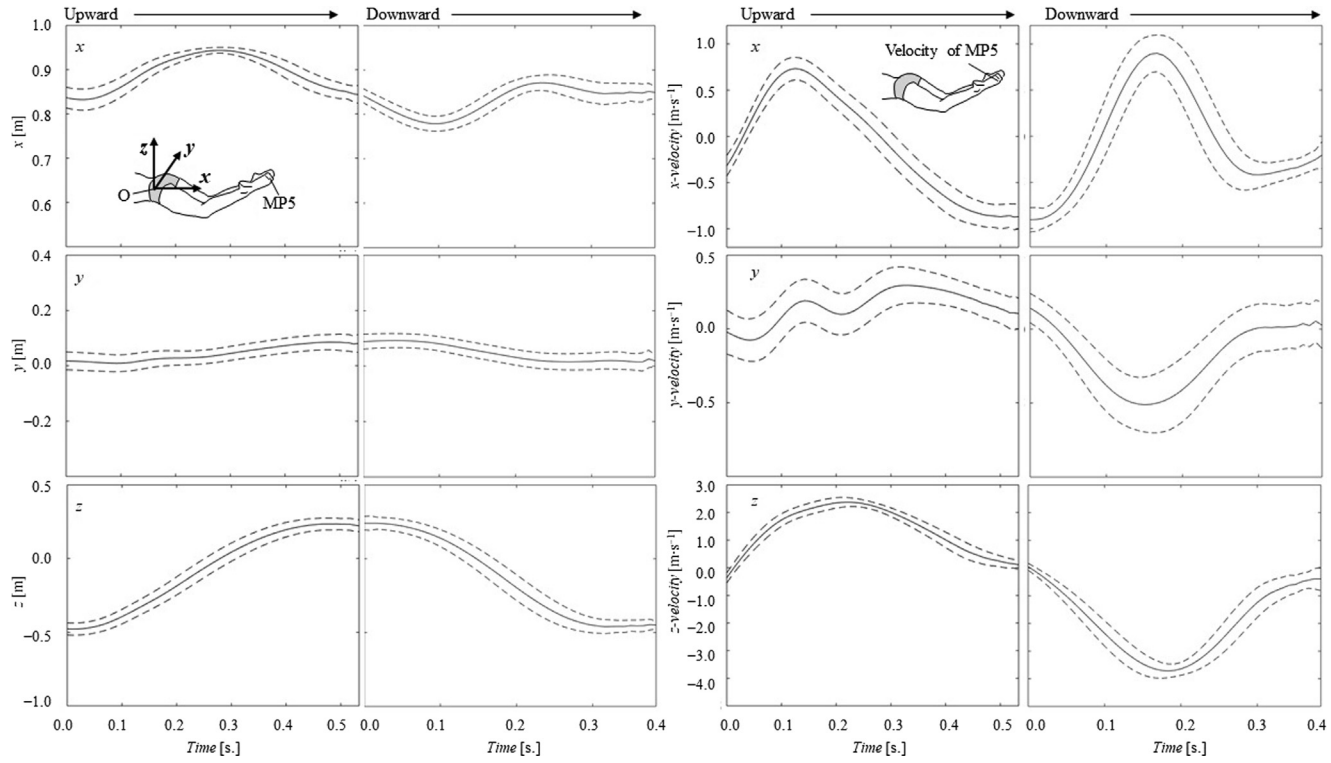

Fig. 4. MP5's average (line) and standard deviation (dotted line) of position (left panel) and velocity (right panel) in local coordinates (positions and velocity) from all trial.

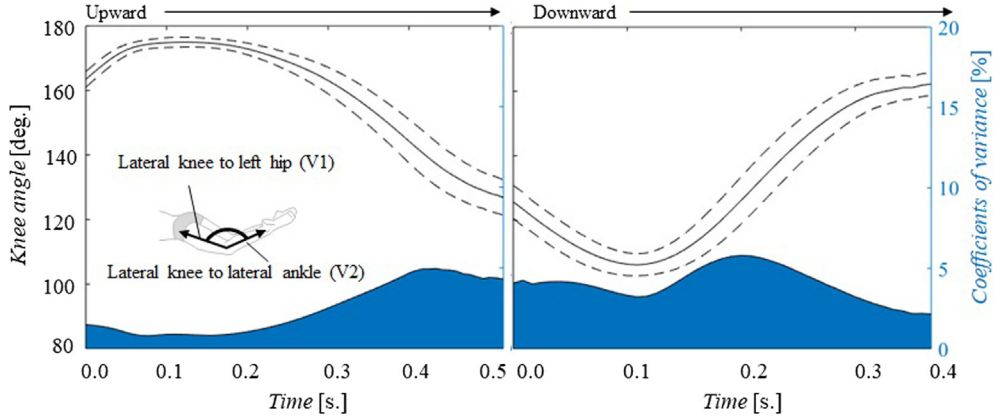

Fig. 5. Average and standard deviation of knee angle from all trial. The knee angle is defined as angle of two vectors (lateral knee to left hip marker V1, and lateral knee to lateral ankle marker V2).

Fig. 6a shows a typical leg motion in the *y*-*z* plane during each phase as well as velocity vectors of the anatomical landmarks and the path of the feet. Specific velocity vectors are observed for the foot at 1st phase of the downward kick, therefore, the foot time sequence of stick images is illustrated in Fig. 6b. The lower limbs moved downward with internal rotations and ankle plantarflexion during the downward kick, and the lower limb external rotation was observed at the end of the downward kick.

Fig. 7 shows the flow fields in the *x*-*z* plane on $y = 0.2$ m. Fig. 8 shows the flow fields in the *y*-*z* plane of flow fields on $x = 1.0$ m. The jet flow was observed after the downward kick (during 1st phase of the downward kick, 1st and 2nd phases of the upward kick), which was released ventral posterior direction. A paired vortex structure was accompanied by jet flow and upstream flow (4th phase of the downward kick and 1st phase of the upward kick in Fig. 6).

Fig. 9 shows the absolute value of the vortices ω in 3D that were isosurfaced, i.e. vortices area were colored by absolute vorticity ($\omega > 0.7\ s^{-1}$; $\omega > 2.0\ s^{-1}$) with typical flow fields. A strong vortex was generated during the downward kick (Fig. 9a). However, the vortex ring structure could not be visualized. A paired vortex was accompanied by an upstream flow at the end of the upward kick (3rd and 4th phases of the upward kick in Fig. 9b).

4. Discussion

The purpose of this study was to visualize the quasi 3D flow field in the wake region during human UUS in a water flume. The jet and the upstream flow structures were observed during downward and upward kicking respectively. These flows induced paired vortices along both sides of the flows. A strong vortex structure was observed during the downward kick.

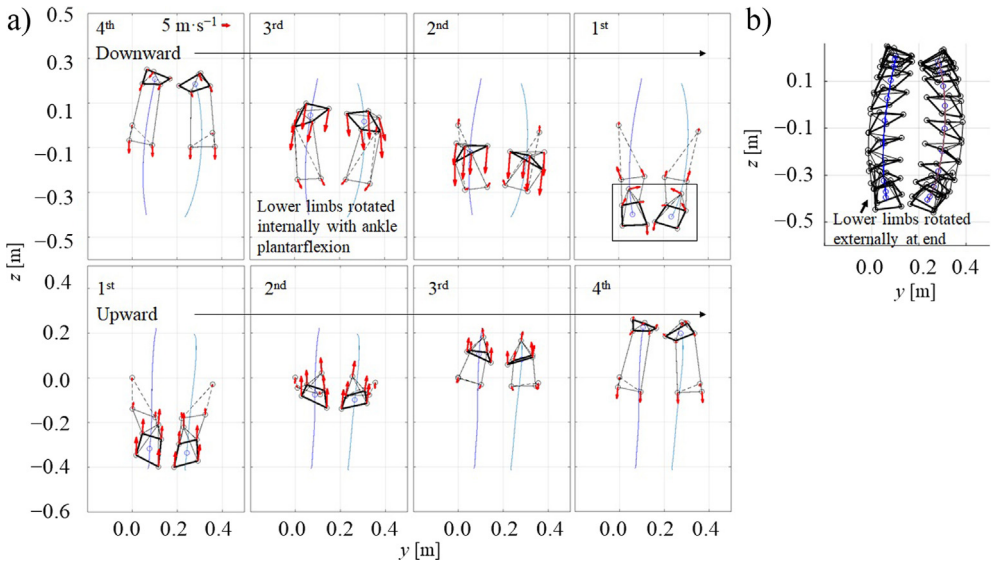

Fig. 6. (a) Typical stick image and velocity vector (not the flow velocity vector) on the anatomical landmarks (red arrow) arranged as actual time order (the downward kick are shown in 4th, 3rd, 2nd, and 1st, the upward kick are shown in 1st, 2nd, 3rd, 4th from left to right panel) at each phase during one kick cycle in the *y*-*z* plane. The thigh (dotted line), shank and heel (solid line), foot (bold line), and the foot pathway (blue line) are illustrated. Specific velocity vectors are observed for the foot at 1st phase of the downward kick (squared line) (b) the foot time sequence of the stick image is shown. The external rotation is observed at the end of the downward kick. (For interpretation of the references to colour in this figure legend, the reader is referred to the web version of this article.)

It is important to discuss the validity of quasi 3D flow field construction in the current study. In this study, the swimmer repeated 41 UUS trials with different positions in the water flume. Previously, the within swimmer variability of skilled swimmers in the vertical undulations of hip, knee, and ankle joints during kick swimming were reported to be 2.3%, 2.8%, and 0.6%, respectively (Sanders, 2007). These values are comparable to the variations of the kinematic variables in this study. This suggests that the effect of fatigue and learning on the repeated motions were small and indicate that the swimmer performed UUS with similar motion in all trials. Besides, to provide high levels of reliability of kinematics of UUS, more than six kick cycles of kinematics data has been required (Connaboy et al., 2010). The averaged flow velocity data was $n_r = 18.3$, i.e. we used 18.3 different kick cycles on average, therefore, it is considered sufficient to establish the reliability of the quasi 3D flow fields for analyzing UUS performance.

The thrust can be estimated by circulation Γ around the vortex and area A surrounded by the vortex (Milne-Thomson, 1966). Ideally, the thrust should be obtained by 3D flow fields to evaluate the actual values of Γ and A without any assumptions (Fish et al., 2014; Flammang et al., 2011). In human UUS, though the errors of predicted drag force in CFD has been reported within a bound of 4% (Bixler et al., 2007), the generation of a vortex ring structure after the downward kick has been visualized in CFD studies (Cohen et al., 2012; Pacholak et al., 2014; von Loebbecke et al., 2009). However, although the measurement volume covered a considerable range in height, i.e. approximately 1.2 m, we could not visualize a vortex ring structure. In fact, researchers visualized vortex ring like structures around swimmers by seeding air bubbles as particles (not PIV) with observation regions set toward the ventral direction of over 1.0 m (Arellano, 1999; Arellano et al., 2002). This might imply that the observation region of PIV measurement must be expanded toward the ventral direction to capture the vortex ring structure in human UUS. In the future, it is necessary to establish a method of quantifying 3D vortex rings, which will enable us to evaluate the thrust and power of the swimmer by only filming.

In human UUS, the propulsion is primarily produced by the downward kick (Cohen et al., 2012). This is due to the restriction of the range of the knee in human (Ungerechts et al., 1998). Our result supports an important role of the downward kick in terms of hydrodynamic structures. Fig. 10 shows a schematic summary of the relationship between fluid dynamics and flow during the downward kick. The present study sheds light on the propulsive mechanism of human UUS such as;

1. During the downward kick, the lower limbs moved downwards with internal rotations and ankle plantarflexion, and the pressure difference between the dorsal and ventral side produces a fluid force (Fig. 10a).
2. The pressure difference produces a leading-edge vortex (LEV) that travels from the ventral to dorsal side of the feet through the toes. After a clock-wise rotating vortex (e.g. left foot) generated by LEV was shed from the foot, it induced a downstream flow (Fig. 10a). The shedding vortices from the feet expanded and created a cluster (1st, 2nd and 3rd phases of the downward kick in Fig. 9a).
3. The swimmer externally rotated his lower limbs at the end of the downward kick, and the toes of the feet approached and then separated each other (Fig. 6). The induced flows collided and formed a strong downward jet flow that gulfed the cluster of shedding vortices as a vortex wake (Fig. 10b), which increased the water momentum in the wake of the swimmer.
4. The cluster of shed vortices and jet flow were released from the feet after the downward kick, and moved toward to the ventral side of the swimmer. (1st and 2nd phases of the upward kick in Fig. 9b).
5. During the upward kick, upstream flow was created with small vortex structure (Fig. 8, Fig. 9b).

5. Limitations

To understand the propulsive mechanism in human UUS, it is ideal to conduct the experiment in static water conditions, i.e. in a swimming pool. However, considering the procedure of quasi 3D flow visualization in this study, it would be unrealistic. For example, we fixed the observation area and required the swimmer to keep the swimming position in the water flume, which enabled

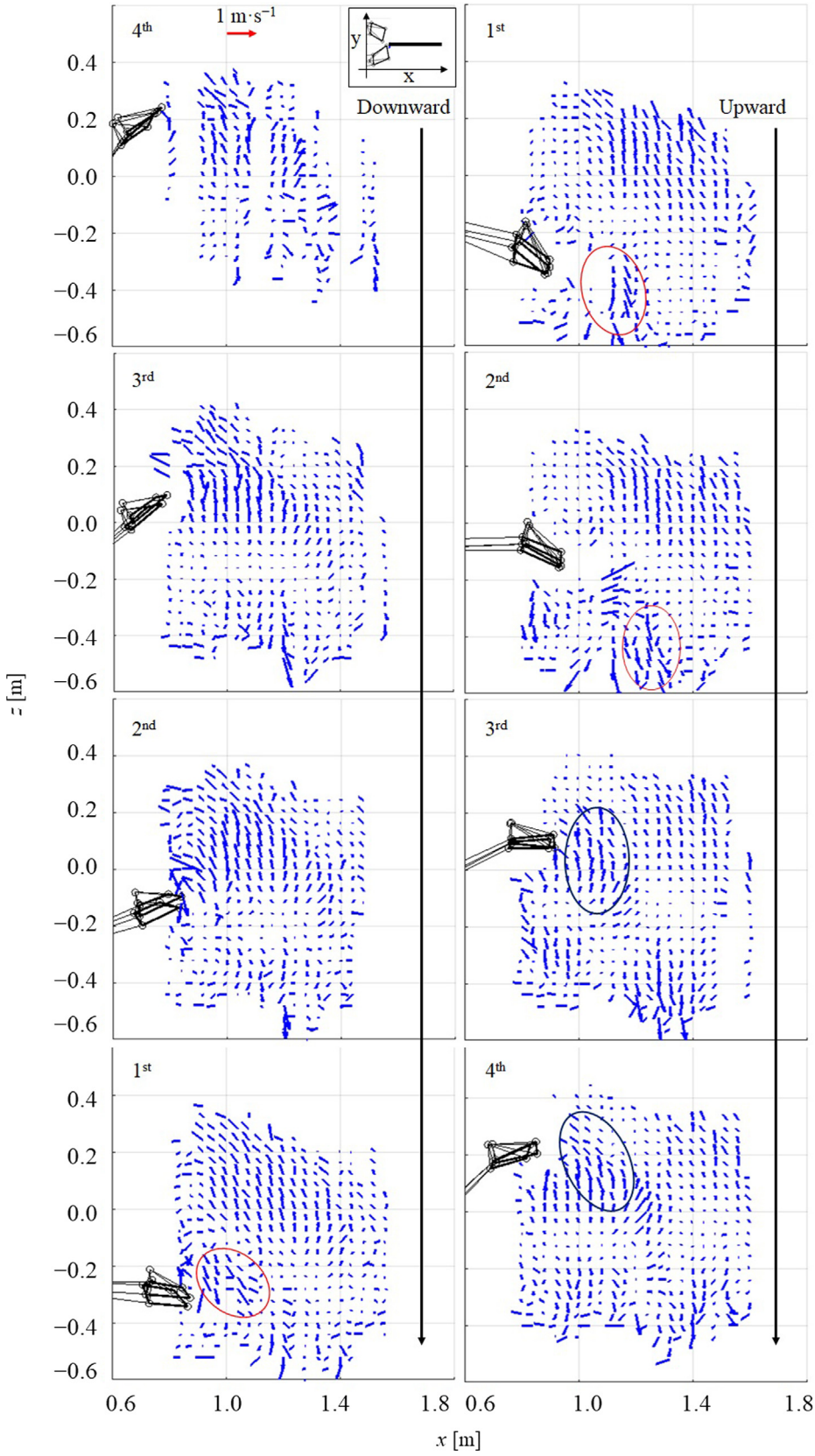

Fig. 7. The spaced flow fields in the *x*-*z* plane on *y* = 0.2 m (center of the swimmer) at each phase arranged as actual time sequences. After the downward kick, the jet is released ventrally and posteriorly (red circle). The upstream flow was observed during the upward kick (circle). (For interpretation of the references to colour in this figure legend, the reader is referred to the web version of this article.)

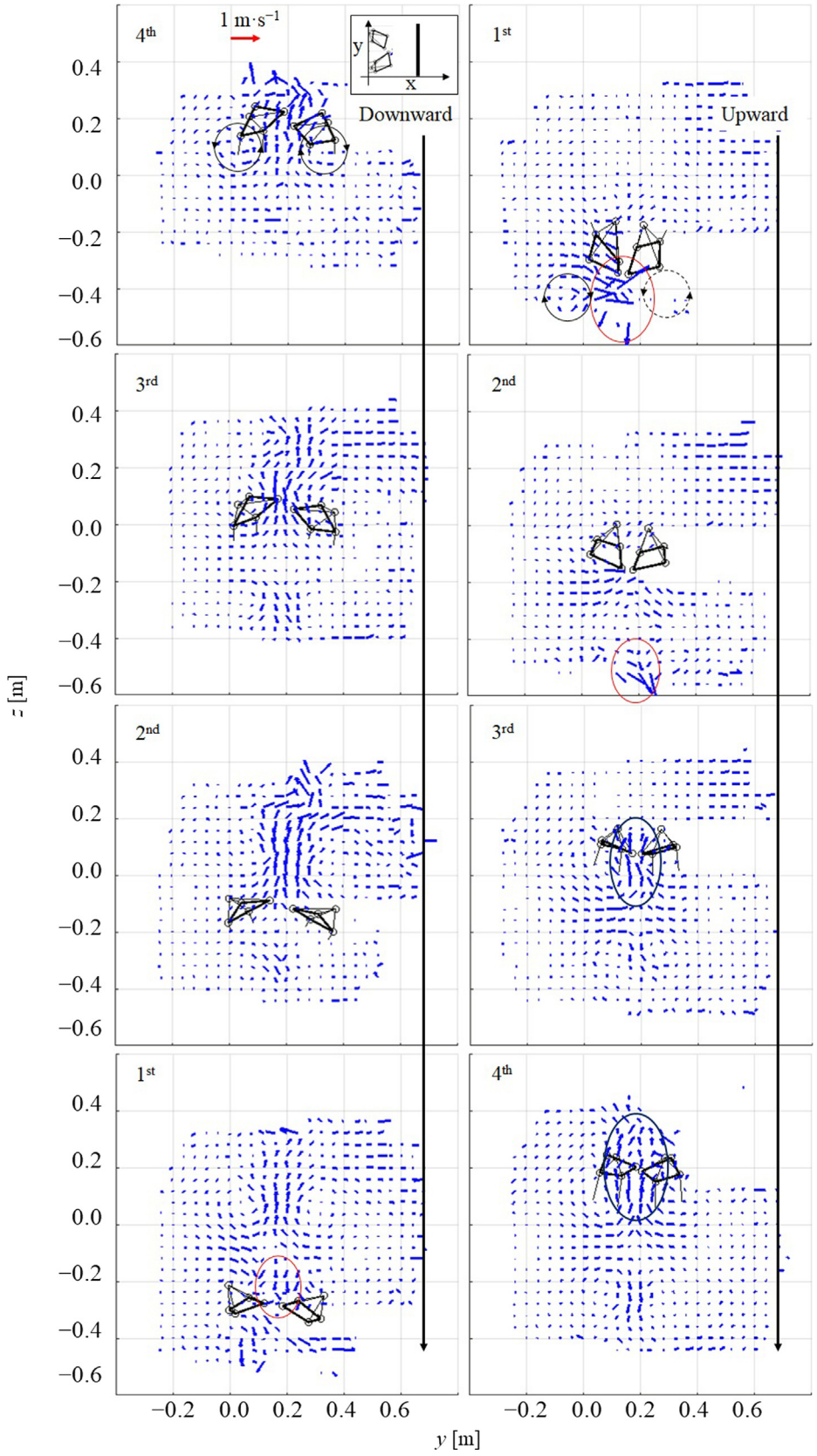

Fig. 8. The spaced flow fields in *y*-*z* plane on *x* = 1.0 m (near the feet) at each phase arranged as actual time sequences. The jet (red circle) and upstream flow (circle) structure are observed also (see Fig. 5), in addition, the paired vortex structure is observed and is accompanied by the jet and the upstream flow in 1st phase of the upward kick and 4th phase of the downward kick respectively. (For interpretation of the references to colour in this figure legend, the reader is referred to the web version of this article.)

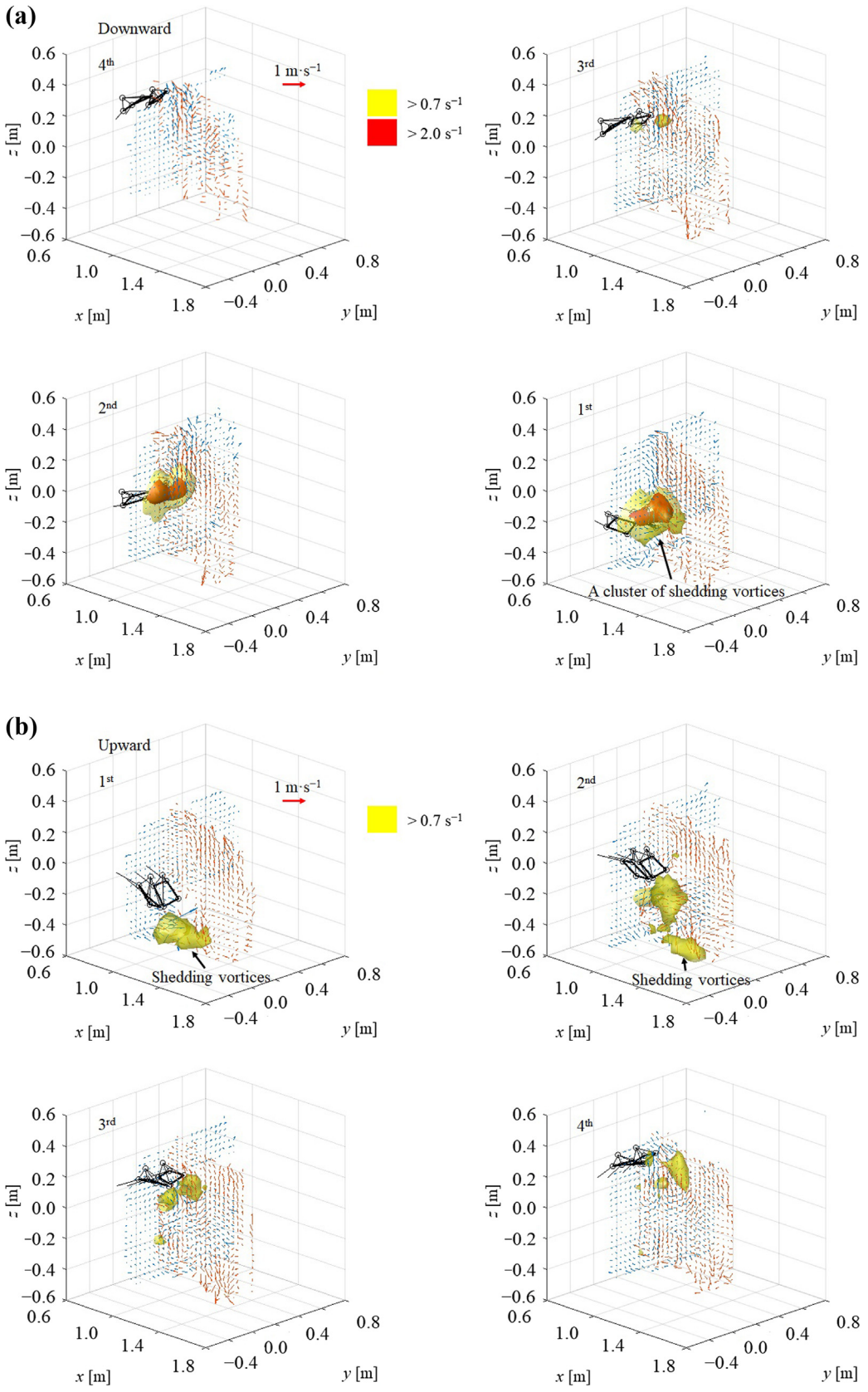

Fig. 9. Three-dimensional vortex structure. The region of generated vortices is isosurfaced, i.e. is colored yellow ($\omega > 0.7\ s^{-1}$) and region of strong vortices are red ($\omega > 2.0\ s^{-1}$). Typical flow fields are illustrated (y-z plane $x = 1.0$ m in blue arrows; x-z plane $y = 0.2$ m in orange arrows; see Figs. 5 and 6) during (a) the downward kick and (b) the upward kick arranged as actual time sequences. (For interpretation of the references to colour in this figure legend, the reader is referred to the web version of this article.)

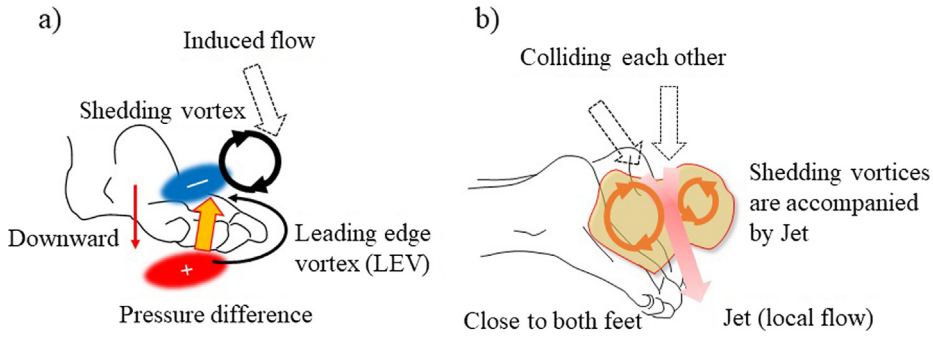

Fig. 10. Schematic summary of kick propulsion mechanics in human UUS. (a) During the downward kick, pressure differences occurred between the dorsal and planter side of the foot (e.g. left foot), which act on the foot as fluid force and a leading-edge vortex (LEV) is formed. The vortex is shed from the foot and it induces downstream flow. (b) The end of the downward kick (4th phase). Both feet approached each other and externally rotate. This induces local flow as a jet that accompanies a strong vortex mass.

many flow fields to be obtained in the cross-sections. This could not be achieved easily in a standard swimming pool.

The flow velocity in the present study was 0.8 $m \cdot s^{-1}$ in the water flume. This velocity was lower than the maximal effort velocity of the swimmer (47.6%) to minimize the fatigue in the repeated trials. Thus, the results explain the propulsive mechanism in a low exercise intensity swimming conditions rather than in competition. The mechanism of human UUS with high swimming velocity would be examined by improving this methodology, for example, extending the intervals between trials for sufficient rest.

6. Conclusion

We visualized the quasi 3D flow fields in wake region during human UUS in a water flume and found that the swimmer externally rotated the lower limbs and the feet moved towards each other at the end of the downward kick. This action generated a strong cluster of vortices and jet flow in the wake resulting in thrust.

Acknowledgements

This work was supported by JSPS KAKENHI, Japan, Grant Number 15H01825, 16 K16540. And this work conducted under Cooperative Research Grant of Advanced Research Initiative for Human High Performance, University of Tsukuba, Japan. The authors also thank Toshihiro Haniu (Kitami Institute of Technology), Ryo Murakawa, and Rina Ebihara (University of Tsukuba) for providing the technical support for the experiment.

Declaration of Competing Interest

Conflict of Interest are none.

Appendix A. Supplementary material

Supplementary data to this article can be found online at https://doi.org/10.1016/j.jbiomech.2019.06.013.

References

Andersen, J.T., Sanders, R.H., 2018. A systematic review of propulsion from the flutter kick – what can we learn from the dolphin kick? J. Sports Sci. 36 (18), 2068–2075.
Arellano, R., 1999. Vortices and Propulsion. Proceedings of the XVII International Symposium on Biomechanics in Sports. University of Western Australia, Perth.
Arellano, R., Pardillo, S., Gavilán, A., 2002. Underwater undulatory swimming: kinematic characteristics, vortex generation and application during the start, turn and swimming strokes. Proceedings of the XXth International Symposium on Biomechanics in Sports. Universidad de Extremadura, Caceras.
Biewener, A.A., 2003. Animal Locomotion. Oxford Animal Biology Series.
Bixler, B., Pease, D., Fairhurst, F., 2007. The accuracy of computational fluid dynamics analysis of the passive drag of a male swimmer. Sports Biomech. 6 (1), 81–98.
Cohen, R.C.Z., Cleary, P.W., Mason, B.R., 2012. Simulations of dolphin kick swimming using smoothed particle hydrodynamics. Hum. Mov. Sci. 31 (3), 604–619.
Connaboy, C., Coleman, S., Moir, G., Sanders, R., 2010. Measures of reliability in the kinematics of maximal undulatory underwater swimming. Med. Sci. Sports Exerc. 42 (4), 762–770.
Connaboy, C., Coleman, S., Sanders, R.H., 2009. Hydrodynamics of undulatory underwater swimming: a review. Sports Biomech. Int. Soc. Biomech. Sports 8 (4), 360–380.
Drucker, Lauder, 1999. Locomotor forces on a swimming fish: three-dimensional vortex wake dynamics quantified using digital particle image velocimetry. J. Experim. Biol. 202 (Pt 18), 2393–2412.
Ferziger, J.H., Perić, M., 2012. Computational methods in fluid dynamics. Springer, Berlin.
Fish, F., Legac, P., Williams, T.M., Wei, T., 2014. Measurement of hydrodynamic force generation by swimming dolphins using bubble DPIV. J. Exp. Biol. 217 (2), 252–260.
Fish, F., Williams, T., Sherman, E., Moon, Y., Wu, V., Wei, T., 2018. Experimental measurement of dolphin thrust generated during a tail stand using DPIV. Fluids 3 (2), 33.
Flammang, B.E., Lauder, G.V., Troolin, D.R., Strand, T.E., 2011. Volumetric imaging of fish locomotion. Biol. Lett. 7 (5), 695–698.
Hart, D.P., 2000. PIV error correction. Exp. Fluids 29 (1), 13–22.
Hochstein, S., Blickhan, R., 2011. Vortex re-capturing and kinematics in human underwater undulatory swimming. Hum. Mov. Sci. 30 (5), 998–1007.
Imamura, N., Matsuuchi, K., 2013. Relationship between vortex ring in tail fin wake and propulsive force. Exp. Fluids 54 (10), 1605.
Matsuuchi, K., Miwa, T., Nomura, T., Sakakibara, J., Shintani, H., Ungerechts, B.E., 2009. Unsteady flow field around a human hand and propulsive force in swimming. J. Biomech. 42 (1), 42–47.
Milne-Thomson, L.M., 1966. Theoretical aerodynamics. Macmillan, New York.
Miwa, T., Matsuuchi, K., Shintani, H., Kamata, E., Nomura, T., 2006. Unsteady flow measurement of dolphin kicking wake in sagittal plane using 2C-PIV. In Proceedings of the Xth Congress of Biomechanics and Medicine in Swimming. Portuguese Journal of Sports Sciences, Portuguese.
Pacholak, S., Hochstein, S., Rudert, A., Brücker, C., 2014. Unsteady flow phenomena in human undulatory swimming: a numerical approach. Sports Biomech. 13 (2), 176–194.
Sakakibara, J., Nakagawa, M., Yoshida, M., 2004. Stereo-PIV study of flow around a maneuvering fish. Exp. Fluids 36 (2), 282–293.
Sanders, R.H., 2007. Kinematics, coordination, variability, and biological noise in the prone flutter kick at different levels of a "learn-to-swim" programme. J. Sports Sci. 25 (2), 213–227.
Tsunokawa, T., Nakashima, M., Takagi, H., 2015. Use of pressure distribution analysis to estimate fluid forces around a foot during breaststroke kicking. Sports Eng. 18 (3), 149–156.
Ungerechts, B.E., Daly, D., Zhu, J.P., 1998. What dolphins tell us about hydrodynamics. J. Swim. Res. 13, 1–7.
von Loebbecke, A., Mittal, R., Mark, R., Hahn, J., 2009. A computational method for analysis of underwater dolphin kick hydrodynamics in human swimming. Sports Biomech. Int. Soc. Biomech Sports 8 (1), 60–77.
Weihs, D., 1972. Semi-infinite vortex trails, and their relation to oscillating airfoils. J. Fluid Mech. 54 (4), 679.